AIP | Applied Physics Letters

Transistor-based metamaterials with dynamically tunable nonlinear susceptibility

John P. Barrett, Alexander R. Katko, and Steven A. Cummer

Citation: Applied Physics Letters **109**, 061901 (2016); doi: 10.1063/1.4960767
View online: http://dx.doi.org/10.1063/1.4960767
View Table of Contents: http://scitation.aip.org/content/aip/journal/apl/109/6?ver=pdfcov
Published by the AIP Publishing

Articles you may be interested in
A frequency and bandwidth tunable metamaterial absorber in x-band
J. Appl. Phys. **117**, 173103 (2015); 10.1063/1.4919753

Mechanically stretchable and tunable metamaterial absorber
Appl. Phys. Lett. **106**, 091907 (2015); 10.1063/1.4914502

Conductive rubber based flexible metamaterial
Appl. Phys. Lett. **106**, 061906 (2015); 10.1063/1.4908253

Time-varying transistor-based metamaterial for tunability, mixing, and efficient phase conjugation
J. Appl. Phys. **115**, 144501 (2014); 10.1063/1.4871195

Ferrite based metamaterials with thermo-tunable negative refractive index
Appl. Phys. Lett. **103**, 131915 (2013); 10.1063/1.4823598

Reuse of AIP Publishing content is subject to the terms at: https://publishing.aip.org/authors/rights-and-permissions. Download to IP: 152.3.34.5 On: Fri, 26 Aug 2016 18:16:51

APPLIED PHYSICS LETTERS **109**, 061901 (2016)

Transistor-based metamaterials with dynamically tunable nonlinear susceptibility

John P. Barrett, Alexander R. Katko,[a)] and Steven A. Cummer[b)]
Department of Electrical and Computer Engineering and Center for Metamaterials and Integrated Plasmonics, Duke University, Durham, North Carolina 27708, USA

(Received 19 April 2016; accepted 29 July 2016; published online 8 August 2016)

We present the design, analysis, and experimental demonstration of an electromagnetic metamaterial with a dynamically tunable effective nonlinear susceptibility. Split-ring resonators loaded with transistors are shown theoretically and experimentally to act as metamaterials with a second-order nonlinear susceptibility that can be adjusted through the use of a bias voltage. Measurements confirm that this allows for the design of a nonlinear metamaterial with adjustable mixing efficiency. *Published by AIP Publishing.* [http://dx.doi.org/10.1063/1.4960767]

Broadly defined as structures with bulk properties different from the properties of their constituent materials, metamaterials have been used to demonstrate a wide variety of interesting and exotic properties including negative index of refraction,[1–3] zero index of refraction,[4] hyperbolic dispersion,[5] and many other results unusual or unattainable with natural materials.[6,7] In turn, metamaterials with these properties have been utilized to design devices with exciting characteristics, such as invisibility cloaks,[8] super-[9,10] or hyperlenses,[11] and time reversal lenses.[12,13] The bulk of the early metamaterial work concentrated on realizing interesting linear effective properties, but recently the focus has shifted to nonlinear properties and active control of metamaterials.

Nonlinear metamaterials have been demonstrated relying on both embedded devices (typically at RF[14,15]) and intrinsically nonlinear materials (typically at higher frequencies). The approach of embedding nonlinear circuit elements at RF has yielded metamaterials with a wide range of useful characteristics, including harmonic generation,[16–18] three- and four-wave mixing,[19–21] phase conjugation,[22] RF limiting,[23] spatiotemporal solitons,[24] and tunable Fano resonance, as well as tunable resonance characteristics based on both DC voltage control[25] and incident power level.[26] The embedded devices at RF have included varactor diodes,[22,26,27] PIN diodes,[23] and MEMS devices.[28] Nonlinear metamaterials can be described by effective nonlinear susceptibilities.[21,29,30] Using varactor diodes, the effective second-order nonlinear susceptibility $\chi_m^{(2)}$ was retrieved and shown to agree with analytical and perturbative approaches.[21,30]

Greater control and a wider range of effective properties can be achieved by moving beyond two-terminal devices. It has been recently shown that using more complex devices such as transistors can improve the performance of a nonlinear metamaterial by increasing its mixing efficiency.[31] In this work, we extend previous work by demonstrating that the use of transistors embedded in metamaterials provide a wide range of realizable nonlinear properties. Using the extra design freedom provided by a transistor, we gain tunability of nonlinear properties as well as linear properties. In particular, we show experimentally that a transistor-embedded split-ring resonator (SRR) can be used to realize a metamaterial with dynamically tunable nonlinear susceptibility.

For this work, we focus on an n-channel MOSFET (specifically the BSS83) as the transistor of choice. There are multiple regions of operation for a MOSFET which depend on the bias conditions at the terminals, which in turn control the effective properties of the transistor. The particular operating region of interest for this work is the subthreshold region in which $V_{GS} < V_T$, where V_T is the threshold voltage and V_{GS} is the gate-source bias. When a transistor is biased in subthreshold, the transistor state has not reached the onset of strong inversion and is either in accumulation, depletion, weak inversion, or moderate inversion.

There are several models for describing the DC characteristics of a transistor operating in the subthreshold region which are helpful in determining the approximate incremental resistance and simplifying the analysis to that of a diode with a tunable reverse saturation current (I_s). The reverse saturation current can change by several orders of magnitude which will help tune the overall nonlinearity of the system. The exponential dependence of I_s on V_{GS} will result in the scaling of each term in the Taylor series expansion of the exponential, resulting in an increase in the generated harmonic currents through the conductive element. However, if the drain-to-source voltage (V_{DS}) is small enough, the primary method of current conduction in the device is capacitive rather than resistive, resulting in the need for developing a small signal model.

The completion of the small-signal behavior within the transistor requires determining all the capacitances that are associated with the MOSFET device. The application of voltages on the various terminals of the MOSFET redistributes charges, essentially making several tunable capacitors. For example, changing V_{GS} will change the charge distribution directly underneath the oxide through the creation of an inversion layer. The capacitances that are caused by this charge redistribution are called intrinsic capacitances and exhibit voltage dependence in very different ways than from a typical varactor diode.[32,33] There are additional capacitances in the transistor device that are directly caused by the physical structure of the device (oxide, diodes, etc.) and are

[a)]Now with Pivotal Communications, Bellevue, WA 98005, USA.
[b)]Electronic mail: cummer@duke.edu

Reuse of AIP Publishing content is subject to the terms at: https://publishing.aip.org/authors/rights-and-permissions. Download to IP: 152.3.34.5 On: Fri, 26 Aug 2016 18:16:51

called extrinsic capacitances which will affect the transistor operation in addition to the intrinsic capacitances.

Based on how the transistor is embedded within the SRR (Fig. 1(a)) and electrically connecting the bulk and source ($V_{DS} = V_{DB}$), we will assume that the primary capacitances (Fig. 1(b)) that will be utilized are the intrinsic bulk to drain capacitance (C_{bd}) and extrinsic capacitance created from the bulk-drain diode (C_{bde}). Both these capacitances are voltage dependent which will result in the generation of harmonics when a single frequency sinusoidal signal is applied. There are other capacitances that will affect the total nonlinearity[32,33] but for this specific transistor configuration in which the drain and source are connected by the SRR loop (Fig. 1), only C_{bd} and C_{bde} will be examined as they will be the dominant capacitances. The calculations for C_{bd} and C_{bde} are shown in the following equations (n is the local sub-threshold slope, C_{ox} is the oxide capacitance, V_T is the threshold voltage, ϕ_t is the thermal voltage, C_0 is the zero bias drain to bulk junction capacitance, V_J is related to the junction built-in voltage, and M is the exponent in which the capacitance changes with reverse voltage).[33]

$$C_{bd}(V_{DB}, V_{GS}) = (n-1)C_{gd}, \tag{1}$$

$$C_{gd}(V_{DB}, V_{GS}) = C_{ox}\left[\frac{1}{C_{gss}(i_r, i_f)} + \frac{1}{C_{gsw}(i_r)}\right]^{-1}, \tag{2}$$

$$C_{gss}(i_r, i_f) = \frac{2}{3}\left[1 - \frac{i_f}{\left(\sqrt{i_r} + \sqrt{i_f}\right)^2}\right], \tag{3}$$

$$C_{gsw}(i_r) = i_r \frac{1}{\sqrt{i_r + \frac{1}{2}\sqrt{i_r} + 1}}, \tag{4}$$

$$i_f(V_P) = \left[\ln\left(1 + e^{\frac{V_P}{2\phi_t}}\right)\right]^2, \tag{5}$$

$$i_r(V_{DB}, V_P) = \left[\ln\left(1 + e^{\frac{V_P - V_{DB}}{2\phi_t}}\right)\right]^2, \tag{6}$$

$$V_P(V_{GS}) = \frac{V_{GS} - V_T}{n}, \tag{7}$$

$$C_{bde}(V_{DB}) = C_0\left(1 + \frac{V_{DB}}{V_J}\right)^{-M}. \tag{8}$$

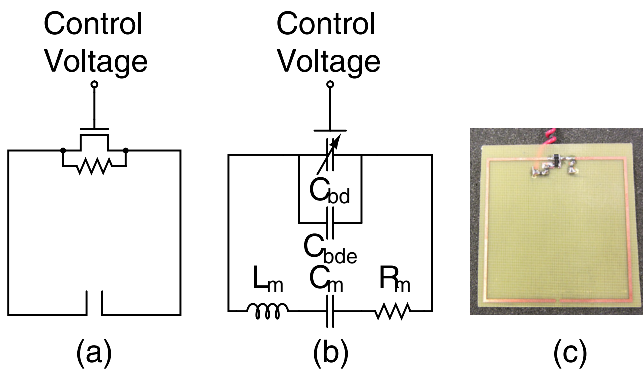

FIG. 1. (a) Schematic, (b) effective circuit model, and (c) fabricated transistor-loaded SRR. In this work, the transistor is operating in the sub-threshold region and V_{DS} is 0 forcing the primary current pathways through the transistor are through the intrinsic (C_{bd}) and extrinsic (C_{bde}) capacitances. The SRR geometry is 4 cm × 4 cm.

To quantify the strength of the generated harmonics and assuming that the signal voltage across the terminals is sufficiently small, C_{bd} and C_{bde} can be expanded around $V_{DS} = 0$ as a Taylor series.

$$C(V_{DS}) = C_0 + C_1 V_{DS} + C_2 V_{DS}^2 + \cdots \tag{9}$$

$$C_n = \frac{1}{n!}\frac{\partial^n C}{\partial V_{DS}{}^n}\bigg|_{V_{DS}=0}. \tag{10}$$

From the frequency domain, the magnitude of current through a capacitor is proportional to the product of the capacitance and the voltage ($I \propto CV$). If $V = V_0 e^{i\omega t}$, then the current equation becomes

$$I \propto C_0 V_0 e^{i\omega t} + C_1 V_0^2 e^{i2\omega t} + \cdots, \tag{11}$$

resulting in the primary coefficient of interest for second harmonic generation being C_1. From the equations for calculating C_{bd} and C_{bde}, C_1 can be determined for varying V_{GS} (Fig. 2). The extrinsic capacitance coefficients are generally independent of V_{GS} (Eq. (8)) but still contribute to the total nonlinear capacitance, setting the minimum amount of nonlinearity in the device. The intrinsic capacitance is the variable element and tunes over a wide range of values but the transistor should be in moderate inversion to attain the maximum value of C_1 and for C_{bd} to have strongest impact on the total capacitance.

The values in Fig. 2 are calculated based upon assumed parameters derived from the measured DC characteristics. The BSS83 does not have a comprehensive Spice model which would give many of the parameters needed for the capacitance calculations. Very precise values of n in Eq. (7) are necessary for the accurate computation of C_{gd} and C_{bd}, which is difficult to achieve unless the surface potential is well known. Therefore, we note that we do not expect to reproduce in the measurement the precise quantitative features of Fig. 2. Essential features, however, are that changing V_{GS} will in turn change the C_1 coefficient in the expanded C_{bd} expression, modulating the generated second harmonic

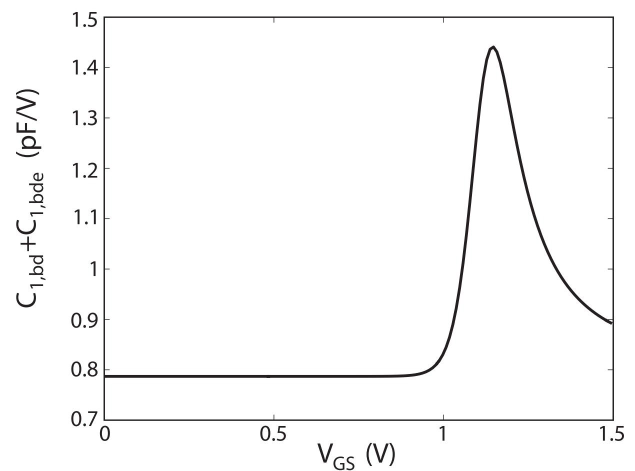

FIG. 2. Calculated first order voltage dependent capacitive (C_1) coefficient for the intrinsic (C_{bd}) and extrinsic (C_{bde}) bulk to drain capacitance for a BSS83 transistor ($C_1 \propto \chi_m^{(2)}$). The parameters for the C_{bd} calculation were extracted using data collected from DC measurements and the parameters for the C_{bde} calculation were provided by the manufacturer.

Reuse of AIP Publishing content is subject to the terms at: https://publishing.aip.org/authors/rights-and-permissions. Download to IP: 152.3.34.5 On: Fri, 26 Aug 2016 18:16:51

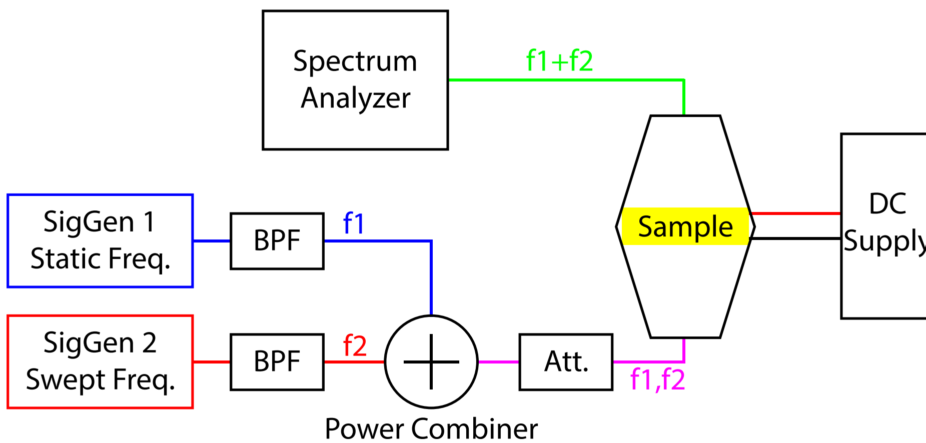

FIG. 3. Block diagram showing experimental setup to retrieve $\chi_m^{(2)}$.

current; that this change comes with a threshold in V_{GS}; and the expected increase in the nonlinear capacitance (which is tied directly to $\chi_m^{(2)}$ is on the order of 50%–100%). This analysis also does not take into account short channel effects which could increase the baseline and change the curvature of C_1 for C_{bd} as well as introduce a voltage-dependent fringing capacitance between the gate and the drain.[32] This fringing capacitance is typically ignored in long-channel MOSFETs but can play a significant role in short channel devices, particularly if the device is biased in depletion or weak inversion.

The experimental verification of the work shown in Ref. 21 was accomplished by examining a three-wave mixing experiment (Fig. 3): two signal generators are used to produce incident fields at frequencies ω_1, ω_2 which are incident on a nonlinear metamaterial. The fields produced at the sum frequency $\omega_s = \omega_1 + \omega_2$ are proportional to the second order nonlinear susceptibility $\chi_m^{(2)}$ for the nonlinear magnetic metamaterial used in the experiment. We conducted a similar experiment for a nonlinear subthreshold transistor metamaterial by sweeping the signal at ω_1 from 500 MHz to 1 GHz while keeping the signal at $\omega_2 = 650$ MHz, near the resonant frequency of the transistor metamaterial. The signal at the sum frequency is measured and converted to the magnetic field value, using

$$H = \sqrt{\frac{2P}{z_0 A}}, \tag{12}$$

where P is the power of the wave, z_0 is the wave impedance in approximately free space (377 Ω), and A is the cross-sectional area of the waveguide, in this case 171.1 cm^2. Following the notation from previous work,[21] $H^+_{3,\exp}$ denotes that the value is experimentally measured after being transmitted through the metamaterial slab and $(\omega_{1,2})$ explains that the measured field is at the sum frequency. This field is directly proportional to the effective $\chi_m^{(2)}$ for the metamaterial.[30] We wish to determine $|H^+_{3,\exp}(\omega_{1,2})|$ as a function of both frequency and V_{GS}. The metamaterial design has been previously described in linear transistor work:[31] a single SRR unit cell with an embedded MOSFET and DC bias lines for the gate to supply a DC V_{GS} (see Fig. 1(c)). The DC bias lines are isolated using very large resistors which can be used since the gate to source current is effectively zero and are configured such that the wires will be perpendicular to the applied electric field component of the incident wave.

We record the generated sum frequency signal as a function of ω_1 and V_{GS}, Fourier process and convert to magnetic field values using Eq. (12). From the magnetic field values, we calculate $\chi_m^{(2)}$ (Fig. 4) using the procedure developed by Rose *et al.*[21] and Larouche *et al.*[30] When the data in Fig. 4 are compared with previous work,[21,30] we see the same qualitative behavior: for any individual value of V_{GS}, the sum frequency field has a maximum value near $2f_{resonant}$. The data from Fig. 4 also confirm that we can adjust V_{GS} to dynamically adjust the effective $\chi_m^{(2)}$ of the metamaterial.

From Fig. 4, the experiments exhibit characteristics that support the analysis summarized in Fig. 2. First, we experimentally observe a V_{GS} threshold below which $\chi_m^{(2)}$ and C_1 are fixed, as predicted by the analysis. Second, both the theory and experiment predict steep increases in $\chi_m^{(2)}$ and C_1 on the order of a factor of two. As expected from not having access to precise parameter values for the calculations, there are a few quantitative differences between the theory and experiment. The theoretical analysis predicted a dramatic increase of the second-order nonlinearity when $V_{M0} < V_{GS} < V_T$, reaching a maximum at $V_{GS} = V_T$. In the measurements, an increase in the second-order nonlinearity was observed starting around $V_{GS} = 0.5$ V (which corresponds approximately to the device entering weak inversion per our assumed parameters) without ever decreasing. The rate of change for both $\chi_m^{(2)}$ and C_1 is different as well with the experimental measurements yielding a $\chi_m^{(2)}$ modulation that is much more gradual than the slope of the calculated C_1.

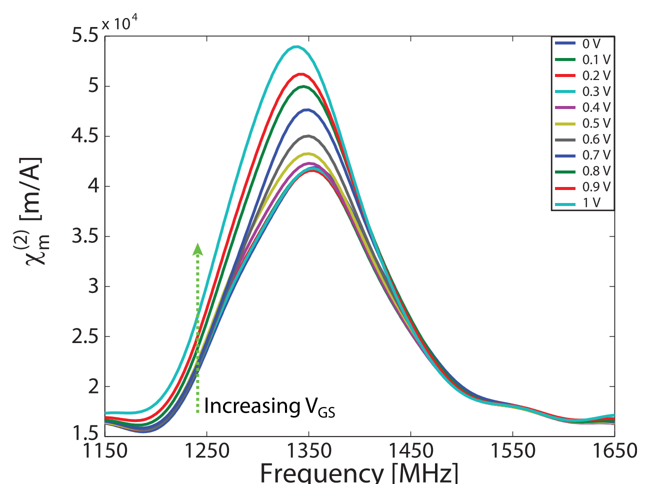

FIG. 4. Measured $\chi_m^{(2)}$ for transistor metamaterial with varying V_{GS}.

Reuse of AIP Publishing content is subject to the terms at: https://publishing.aip.org/authors/rights-and-permissions. Download to IP: 152.3.34.5 On: Fri, 26 Aug 2016 18:16:51

These discrepancies are likely explained by our assumption regarding the simplification of the transistor model in Fig. 1. The main assumptions needed to complete the calculations required the gate be completely isolated from the drain and source and that the device was long channel. In real devices, the extrinsic capacitances between the drain/source and gate will cause coupling between the terminals and generate a small voltage on the gate. This gate voltage will in turn cause additional charge redistribution as well as bring the nonlinear components of the gate-to-bulk capacitance C_{gb} into the model. The previously mentioned short channel effects can also change the extrinsic gate to drain capacitance from a simple linear capacitance to a nonlinear capacitance in itself, which will also introduce additional nonlinearity. An additional minor difference between the $\chi_m^{(2)}$ and C_1 curves refers to the maximum observed in the calculations while not being observed in the measurements. This is simply due to the fact that V_{GS} in the measurements was always below V_T ($\approx$1.15 V).

We also note that the measured $\chi_m^{(2)}$ values in Fig. 4 are significantly larger than the previously reported values for varactor-base nonlinear metamaterials.[21,30] There are several reasons for this. The material nonlinearity can be tuned by manipulating the parameters in the calculation of $\chi_m^{(2)} = I^{(2)}A/(VH^2)$ where $I^{(2)}$ is the generated second harmonic current, A is the loop area, V is the unit cell volume, and H is the incident magnetic flux. The unit cell used in this work has a loop area that is 50 times larger than the area for the unit cell described in Refs. 21 and 30, corresponding to an induced voltage that is 50 times higher which leads to a significant increase in effective V_{DS}. The bulk-drain diode parameters also affect the second-order nonlinearity through variations in the M and V_J from Eq. (8). Combining these effects of increased SRR loop area, varied structure capacitance nonlinearity, and the effective conductance tunability, this increase in second-order nonlinearity is expected.

In summary, this work demonstrates a metamaterial with tunable nonlinear susceptance. Metamaterials using varactor diodes, as in Ref. 30, present an effective $\chi_m^{(2)}$. However, in order to modulate the $\chi_m^{(2)}$ of the metamaterial, it is necessary to alter the characteristics of the charge distribution within the diode element. By using a transistor, we are able to change the reactive and resistive characteristics of a nonlinear metamaterial electrically utilizing the additional terminals. By biasing the device in the subthreshold region, the effective $\chi_m^{(2)}$ of a material can be tuned over a significant range. Control of the nonlinearity can increase the design space for metamaterials by introducing a way to engineer a material based upon desired nonlinear, in addition to linear, characteristics. Future work includes the expansion of the models based on Enz-Krummenacher-Vittoz (EKV) theory using harmonic balance-based simulators as well as potential applications in the development of mixers tunable mixing efficiency and components in the field of nonlinear optics.

This work was supported by a Multidisciplinary University Research Initiative from the Army Research Office (Contract No. W911NF-09-1-0539).

[1] V. Veselago, Sov. Phys. - Usp. **10**, 509 (1968).
[2] R. Shelby, D. Smith, and S. Schultz, Science **292**, 77 (2001).
[3] D. R. Smith, W. J. Padilla, D. C. Vier, S. C. Nemat-Nasser, and S. Schultz, Phys. Rev. Lett. **84**, 4184 (2000).
[4] R. Ziolkowski, Phys. Rev. E **70**, 046608 (2004).
[5] M. A. Noginov, Y. A. Barnakov, G. Zhu, T. Tumkur, H. Li, and E. E. Narimanov, Appl. Phys. Lett. **94**, 151105 (2009).
[6] J. Pendry, A. Holden, D. Robbins, and W. Stewart, IEEE Trans. Microwave Theory Tech. **47**, 2075 (1999).
[7] D. Schurig, J. Mock, and D. Smith, Appl. Phys. Lett. **88**, 041109 (2006).
[8] D. Schurig, J. J. Mock, B. J. Justice, S. A. Cummer, J. B. Pendry, A. F. Starr, and D. R. Smith, Science **314**, 977 (2006).
[9] J. Pendry, Phys. Rev. Lett. **85**, 3966 (2000).
[10] N. Fang, H. Lee, C. Sun, and X. Zhang, Science **308**, 534 (2005).
[11] Z. Liu, H. Lee, Y. Xiong, C. Sun, and X. Zhang, Science **315**, 1686 (2007).
[12] S. Maslovski and S. Tretyakov, J. Appl. Phys. **94**, 4241 (2003).
[13] J. Pendry, Science **322**, 71 (2008).
[14] A. Katko, B.-I. Popa, J. Barrett, A. Hawkes, and S. Cummer, Proc. SPIE **8093**, 809309 (2011).
[15] A. Katko, A. Hawkes, and S. Cummer, Proc. SPIE **8455**, 84550B (2012).
[16] I. Shadrivov, A. Kozyrev, D. van der Weide, and Y. Kivshar, Appl. Phys. Lett. **93**, 161903 (2008).
[17] M. Klein, C. Enkrich, M. Wegener, and S. Linden, Science **313**, 502 (2006).
[18] M. Klein, M. Wegener, N. Feth, and S. Linden, Opt. Express **15**, 5238 (2007).
[19] M. Lapine and M. Gorkunov, Phys. Rev. E **70**, 066601 (2004).
[20] D. Huang, A. Rose, E. Poutrina, S. Larouche, and D. Smith, Appl. Phys. Lett. **98**, 204102 (2011).
[21] A. Rose, S. Larouche, D. Huang, E. Poutrina, and D. Smith, Phys. Rev. E **82**, 036608 (2010).
[22] A. Katko, S. Gu, J. Barrett, B.-I. Popa, G. Shvets, and S. Cummer, Phys. Rev. Lett. **105**, 123905 (2010).
[23] A. Katko, A. Hawkes, J. Barrett, and S. Cummer, IEEE Antennas Wireless Propag. Lett. **10**, 1571 (2011).
[24] I. V. Shadrivov, N. A. Zharova, A. A. Zharov, and Y. S. Kivshar, Opt. Express **13**, 1291 (2005).
[25] I. Shadrivov, S. Morrison, and Y. Kivshar, Opt. Express **14**, 9344 (2006).
[26] A. Slobozhanyuk, P. Kapitanova, I. Shadrivov, P. Belov, and Y. Kivshar, JETP Lett. **95**, 613 (2012).
[27] D. Powell, I. Shadrivov, and Y. Kivshar, Appl. Phys. Lett. **95**, 084102 (2009).
[28] T. Hand and S. Cummer, IEEE Antennas Wireless Propag. Lett. **6**, 401 (2007).
[29] M. Lapine, M. Gorkunov, and K. H. Ringhofer, Phys. Rev. E **67**, 065601 (2003).
[30] S. Larouche, A. Rose, E. Poutrina, D. Huang, and D. Smith, Appl. Phys. Lett. **97**, 011109 (2010).
[31] A. R. Katko, J. P. Barrett, and S. A. Cummer, J. Appl. Phys. **115**, 144501 (2014).
[32] Y. Tsividis, *Operation and Modeling of the MOS Transistor*, 2nd ed. (Oxford University Press, 1999).
[33] C. C. Enz, F. Krummenacher, and E. A. Vittoz, Analog Integr. Circuits Signal Process. **8**, 83 (1995).

Reuse of AIP Publishing content is subject to the terms at: https://publishing.aip.org/authors/rights-and-permissions. Download to IP: 152.3.34.5 On: Fri, 26 Aug 2016 18:16:51